RSC Advances

PAPER

View Article Online
View Journal | View Issue

Cite this: *RSC Adv.*, 2021, **11**, 39246

Tuning the charge transfer and optoelectronic properties of tetrathiafulvalene based organic dye-sensitized solar cells: a theoretical approach†

Smiti Rani Bora and Dhruba Jyoti Kalita *

Here, we have designed a series of dyes following the donor–π–acceptor (D–π–A) architecture by incorporating tetrathiafulvalene (TTF) as the donor unit and phthalazine (PTZ), diketopyrrolopyrrole (DPP) and quinoxaline (QNX) as the acceptor units, along with the thiophene unit as a π-bridge. The designed dyes have been designated as TTF-PTZ, TTF-DPP and TTF-QNX respectively. We have used cyanoacrylic acid as the anchoring group for the dyes TTF-PTZ and TTF-DPP, while for the third dye, TTF-QNX, we used a carboxylic group. The structural, electronic and photochemical properties of the designed dyes are investigated under the regime of density functional theory (DFT) and time-dependent density functional theory (TD-DFT) methods. In this regard, the dihedral angle, energies of the highest occupied molecular orbital (HOMO) and lowest unoccupied molecular orbital (LUMO), energy difference between the HOMO and LUMO (Δ_{H-L} values), partial density of states (PDOS), ground state oxidation potential (GSOP), excited state oxidation potential (ESOP), ionization potential (IP), electron affinity (EA), molecular electrostatic potential surface (MEPS) analysis, reorganization energy (λ), electronic coupling matrix element (V), charge transfer rate (k_{CT}), hopping mobility (μ_{hop}), absorption spectra, exciton binding energy (EBE) and electron density difference (EDD) of the designed dyes are calculated. This study reveals that the dyes TTF-DPP-4 and TTF-DPP-6′ exhibit the lowest Δ_{H-L} values. The study also reveals that the attachment of the $-NH_2$ group at the donor unit and the $-NO_2$ and $-CF_3$ groups at the acceptor units lower the Δ_{H-L} values of all of the designed dyes. We have also observed that the GSOP of all the designed dyes lie below the redox potential of the I^-/I_3^- electrolyte couple. However, the ESOP of the TTF-PTZ and TTF-QNX groups of dyes, along with the most of the dyes belonging to the TTF-DPP group, lie above the conduction band of the TiO_2 semiconducting surface. Moreover, the total reorganization energy (λ_{tot}) values are low for the TTF-DPP and TTF-QNX groups of dyes, which confirm the better electron–hole separation efficiency in these groups of dyes. Furthermore, the absorption properties of the designed dyes indicate that the TTF-DPP groups of dyes possess the maximum absorption wavelength (λ_{max}) values and attachment of the $-CH_3$ group at the donor part increases the electron density of the dyes, which in turn results into the maximum red-shift. Therefore, the study reveals that the designed dyes are likely to exhibit facile charge transport. Moreover, the electronic properties of the dye–TiO_2 clusters strengthen the performance of the dyes compared to those of the isolated dyes. Hence, our study provides good recommendations for the further design of dyes to enhance the performance of dye-sensitized solar cells (DSSCs).

Received 3rd August 2021
Accepted 23rd November 2021

DOI: 10.1039/d1ra05887h

rsc.li/rsc-advances

1. Introduction

Since 1991, the discovery of dye-sensitized solar cells (DSSCs) by O'Regan and Grätzel has attracted the attention researchers due to their improvements in comparison to all other kinds of solar cells.[1,2] DSSCs, as third-generation low cost solar cells, have several advantages over silicon based counterparts, *viz.*, they are thin wafers, free of any toxicity from metals, cost-effective, have prolonged stability and, above all, work well even in diffused light.[3] Several recent crucial advances in the design of dyes for DSSCs have led scientists to compute their power conversion efficiencies (PCEs).[2] A DSSC is basically semiconductor which is

Department of Chemistry, Gauhati University, Guwahati-781014, India. E-mail: dhrubajyoti.kalita@gauhati.ac.in

† Electronic supplementary information (ESI) available: *XYZ* coordinates of the designed dyes, optimized geometries of the designed dyes, optimized structure of the test compound, calculated energies of HOMO and LUMO, Δ_{H-L} and λ_{max} values of the reference compound studied with different functionals, PDOS spectra of the substituted dyes, spectral data of the designed dyes obtained from the PDOS spectra, optimized structure of the stacked unsubstituted dyes, EDD maps of the substituted dyes, PDOS spectra of the substituted dye–Ti_5O_{10} clusters, spectral data of dye–Ti_5O_{10} clusters obtained from the PDOS spectra, MEPS contour plot of the substituted dye–Ti_5O_{10} clusters and EDD maps for the substituted dye–Ti_5O_{10} clusters. See DOI: 10.1039/d1ra05887h

formed between a photo-sensitized anode and an electrolyte. Research has been done in numerous areas for improving the efficiency of DSSCs by modifying electrodes, photosensitizers and electrolytes. Various structural modifications have been performed by synthesizing many new organic photosensitizers which can absorb light in the higher wavelength range and exhibit higher power conversion efficiencies. Grätzel's achievement of 7% efficiency has attracted various researchers to explore DSSCs.[4] In order to serve as a suitable dye for application in DSSCs, the dye must possess certain properties, such as high photo and thermal stability,[5] good adsorption on the semiconducting surface through anchoring groups, high solubility in the solvent, no toxicity, a broad absorption spectrum in the visible range for capturing solar radiation and a suitably high redox potential for dye regeneration following excitation.[6]

Generally, a DSSC consists of an organic dye-sensitizer, mesoporous TiO_2 nanocrystal layers, a photoanode, a counter conducting electrode and an electrolyte (usually the redox iodide/triiodide couple (I^-/I_3^-)). The organic dye-sensitizer and the mesoporous TiO_2 nanocrystal layers are considered to be the dominant constituents for excellent PCEs. Besides TiO_2, the use of SnO_2 and ZnO has also been encouraging as semiconducting surface for the dyes.[7,8] Moreover, one of the main requirements to serve as a suitable dye in DSSCs is to have anchoring groups. Two traditionally employed dye anchoring groups include carboxylic acid and cyanoacrylic acid groups. These groups act as anchors and enable the adsorption of the dye onto a metal oxide substrate.[9] The photosensitizer absorbs the incident photon and undergoes excitation from the ground state (S) to the excited state (S*) of the dye. The excited electrons are injected into the conduction band of the nanoporous TiO_2 electrode, resulting in the oxidation of the photosensitizer (S^+). The injected electrons are thereafter transported between TiO_2 nanoparticles and diffuse toward the back contact (transparent conducting oxide [TCO]). Then, the electrons finally reach the counter electrode through the external circuit. The electrons at the counter electrode reduce I_3^- to I^-. Thus, dye regeneration takes place due to the acceptance of electrons from the I^- ion redox mediator. As a result, I^- gets oxidized to I_3^-. Alongside this, the oxidized mediator (I_3^-) diffuses towards the counter electrode and get reduced to I^-.[10] It is to be noted that the electron injection and dye regeneration processes are two important steps behind the working of a photovoltaic device. These two steps will be possible only when the highest occupied molecular orbital (HOMO) of the sensitizer lies below the chemical potential of the redox couple and the lowest unoccupied molecular orbital (LUMO) of the sensitizer lies above the conduction band (CB) of the semiconductor. The CB of TiO_2 lies at −4.00 eV and the chemical potential of the I^-/I_3^- couple is −4.80 eV. In addition, for an efficient DSSC, the sensitizer must possesses a high oscillator strength, a low band gap, a long-lived excited state and must absorb a broad range of the UV–visible spectrum.

It has been observed that the HOMO and LUMO energy levels can be effectively tuned by molecular engineering. In 2010, Teng *et al.* illustrated that addition of Li^+ ions to the electrolyte brought about an increase in the short circuit current density (J_{SC}) and a decrease in open-circuit voltage (V_{OC}). They also reported that use of Br^-/Br_3^- instead of I^-/I_3^- leads to better power conversion efficiency (PCE).[11] Moreover, it has been already reported that appropriate structural modifications by incorporating various substituents can effectively tune the optoelectronic properties of the dyes. The incorporation of the hydrophobic alkyl groups to the donor or to the π-spacer optimizes the electron transfer rate from the TiO_2 semiconducting surface to the redox medium and thereby renders better efficiency to the dye.[11,12] In the same fashion, dyes with the more electron donating substituents, *viz.*, alkoxy groups and amino groups, are expected to have lower band-gap values.

According to literature, the best model for metal-free organic dye-sensitizers is the donor–π–acceptor (D–π–A) model due to the effective photoinduced intramolecular charge transfer (ICT) in them.[13,14] The D–π–A model helps the dye-sensitizer in tailoring various parameters, such as the ionization potentials (IP), electron affinities (EA),[15,16] absorption properties, difference between the energies of the HOMO and LUMO (Δ_{H-L} values),[16] reorganization energies (λ), charge transfer rates (k_{CT}) *etc.* For effective charge transport, the selection of appropriate pairs of electron donors and acceptors is considered to be the most crucial step in the better management of the optoelectronic properties of the dyes. Molecular dyes showing a wide range of absorption in the visible region and containing anchoring groups, such as cyanoacrylic acid, carboxylic group, or phosphonic acid, serve as excellent candidates for sensitizers. A number of novel metal-free DSSCs based on triphenylamine,[17] coumarin,[18] tetrathiafulvalene,[19] merocyanine,[20] cyanine,[21] indoline,[22] hemicyanin,[23] perylene,[24] oligoene,[25] dialkylaniline,[26] phenothiazine,[27] tetrahydroquinoline[28] and carbazole[29] have been devised with PCEs exceeding 9%. Out of the various novel metal-free DSSCs, tetrathiafulvalene (TTF) based metal-free DSSCs have attracted most researchers in the field of molecular optoelectronics.[30] Tetrathiafulvalene (TTF) is an attractive and strong π-electron donor due to its electrochemical and optical properties, which are finely tunable and thereby induce efficient ICT transitions.[31] In 2010, a group of scientists reported the efficiency of π-extended TTF-derivatives (ex-TTF) in the field of DSSCs as only 3.8% due to the less effective charge-separation and thermodynamically unfavourable HOMO levels which made the dye-regeneration process thermodynamically not feasible.[32] Then, in 2012, another group of scientists worked on dithiafulvalene-based dyes and achieved a better efficiency of 8.3%.[33] Another study has been reported by Lingamallu and co-workers where they synthesized four different D–π–A systems with ex-TTF scaffolds in combination with long alkyl chains and different π-linkers and achieved an overall efficiency of 7.15%.[34] Furthermore, they experimented with another set of dyes in which they switched to different combinations of π-spacers and anchoring groups and obtained efficiencies ranging from 4.55% to 6.36%.[35] In addition to the molecular engineering of donors, the proper selection of suitable acceptors is crucial for the D–π–A model. Within the acceptor library, phthalazine (PTZ), diketopyrollopyrolle (DPP)[36] and quinoxaline (QNX)[37] have emerged as effective electron-

deficient building blocks of low band gap conjugated organic molecules for DSSCs.

In this work, we have designed three different dye-sensitizers based on the D–π–A approach. We have used tetrathiafulvalene (TTF) as the donor unit and substituted the acceptor unit by phthalazine (PTZ), diketopyrollopyrolle (DPP) and quinoxaline (QNX) for the three designed dyes. The three designed dyes have been designated as TTF-PTZ, TTF-DPP and TTF-QNX, respectively. Both the donor and the acceptor units are flanked by a thiophene unit as the π-bridge. The thiophene ring as a π-bridge increases the planarity of the polymeric backbone. We have also used cyanoacrylic acid as the anchoring group for the dyes TTF-PTZ and TTF-DPP, while for the third dye TTF-QNX, it is carboxylic group. Here, we have used TiO_2 as the semiconducting surface. The optimized geometries of the designed dyes are presented in Fig. S1 (in the ESI†) and their structures are presented in Fig. 1.

In order to tune the performance of DSSCs, we have incorporated five electron donating groups, *viz.*, $-CH_3$, $-SC_3H_7$, $-OC_3H_7$, $-NH_2$ and –OH, and three electron withdrawing groups, *viz.*, $-NO_2$, –F and $-CF_3$, at the donor and acceptor units, respectively. These groups are denoted numerically in suffix as 1, 2, 3, 4 and 5 for $-CH_3$, $-SC_3H_7$, $-OC_3H_7$, $-NH_2$ and –OH groups, respectively, and 6′, 7′ and 8′ for $-NO_2$, –F and $-CF_3$ groups, respectively, after the name of their parent dye. The symbol prime (′) is used to indicate that the substituents are attached to the acceptor moiety. The coordinates of the studied compounds are provided in Table S1 (in the ESI†).

2. Validation of the applied methodology

To validate the functionals used in the calculations, we have carried out an extensive study to improve the accuracy of the results. We have performed a test calculation with a quinoxaline-fused tetrathiafulvalene-based sensitizer reported in the literature as it possesses structural similarity with our designed dyes.[19] We have presented the optimized structure of the test compound in Fig. S2 (in the ESI†). The ground state calculations have been performed using six different functionals, *viz.*, B3LYP/6-31G(d), B3LYP-D3/6-31G(d), B3PW91/6-31G(d), CAM-B3LYP/6-31G(d), HSEH1PBE/6-31G(d) and wB97XD/6-31G(d), applying the density functional theory (DFT) method. However, for the excited state calculations, we have performed time-dependent density functional theory (TD-DFT) using the functionals B3LYP/6-31G(d), B3LYP-D3/6-31G(d), B3PW91/6-31G(d), CAM-B3LYP/6-31G(d), HSEH1PBE/6-31G(d) and wB97XD/6-31G(d). We have correlated the calculated energies of the HOMO and LUMO, Δ_{H-L} and λ_{max} with the experimental results. The results are reported in Table S2 (in the ESI†). From this table, it is observed that, for the ground state calculations, the values obtained using the functionals B3LYP/6-31G(d), B3LYP-D3/6-31G(d) and B3PW91/6-31G(d) agree well with the experimental values. On the other hand, for the excited state calculations, the results obtained using the functionals B3LYP/6-31G(d), B3LYP-D3/6-31G(d) and CAM-B3LYP/6-31G(d) are in better agreement with the experimentally reported values. However, to keep the computational cost under control, we have performed the ground state calculations at the B3LYP/6-31G(d) level of theory. On the other hand, we have performed the excited state calculations at the CAM-B3LYP/6-31G(d) level of theory.

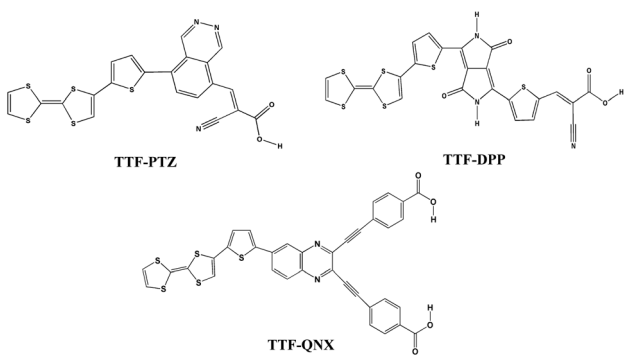

Fig. 1 Structures of the designed dyes.

3. Theoretical methodology

To have a detailed view of the structural, electronic and optical properties of the designed dyes, molecular calculations have been carried out with the Gaussian 09 program package.[38] Geometric optimization has been carried out with the DFT method by employing the B3LYP functional and 6-31G(d) basis set. For the excited state calculations, we have carried out TD-DFT calculations with the ground state optimized geometry of the dyes using the long range corrected functional (*i.e.*, CAM-B3LYP) along with the same basis set. We have covered a range of the 30 lowest singlet–singlet transitions. The optimization of the dye–TiO_2 clusters has been carried out by employing the B3LYP functional along with the LANL2DZ basis set.

The dihedral angle (ϕ) is defined as the angle between the repeating units of the π-conjugated system. It is one of the most important parameters affecting the planarity of the molecules.[39] It significantly affects the conjugation of the polymers, which in turn will affect the optoelectronic properties. It also contributes significantly to the determination of the reorganization energy (λ) and charge transport processes.[40]

The energy band gap (Δ_{H-L}) of the organic dyes is defined as the energy difference between their frontier molecular orbitals, *viz.*, the highest occupied molecular orbital (HOMO) and lowest unoccupied molecular orbital (LUMO). A lower value of the HOMO–LUMO gap facilitates better excitation of the organic dyes. Moreover, smaller HOMO–LUMO gaps correspond to better stability of the organic dyes.

The ionization potential (IP) is defined as the energy required to remove an electron from the neutral species of a molecule. On the other hand, electron affinity (EA) is defined as the difference between the energies of the neutral species and the anion species of a molecule in their lowest energy states.[40–42] We have calculated the IPs and the EAs of the designed dyes using eqn (1) and (2), respectively. These two

parameters help in calculating the efficiency of the designed dyes based on the DFT model.[43]

$$\mathrm{IP} = E^{+}(\mathrm{M}^{\circ}) - E^{\circ}(\mathrm{M}^{\circ}), \quad (1)$$

$$\mathrm{EA} = E^{\circ}(\mathrm{M}^{\circ}) - E^{-}(\mathrm{M}^{\circ}), \quad (2)$$

where E°, E^{+} and E^{-} are the energies of the dyes in the neutral, cationic and anionic states, respectively, and M° represents the neutral geometry of the dyes.

The reorganization energy (λ) can be defined as the change in energy due to the structural reorganization of the dye molecule to minimize the effect of its excess charge.[39] λ usually has two contributions, the outer sphere and the inner sphere. The outer sphere part arises from the relaxation of electrons/nuclei or polarization of the surrounding medium and the inner sphere part arises from the geometric relaxation process, which is associated with the charge acceptance or release by the dye molecule. We have taken into account only the λ values contributed from the inner sphere part. The λ values for the cationic species (λ_{+}) and anionic species (λ_{-}) can be calculated by using eqn (3) and (4), respectively.[43]

$$\lambda_{+} = [E^{+}(\mathrm{M}^{\circ}) - E^{\circ}(\mathrm{M}^{\circ})] - [E^{+}(\mathrm{M}^{+}) - E^{\circ}(\mathrm{M}^{+})], \quad (3)$$

$$\lambda_{-} = [E^{\circ}(\mathrm{M}^{-}) - E^{-}(\mathrm{M}^{-})] - [E^{\circ}(\mathrm{M}^{\circ}) - E^{-}(\mathrm{M}^{\circ})]. \quad (4)$$

Here, M^{+} and M^{-} represent the cationic and anionic geometries of the dyes, respectively.

The energy conversion efficiency (η) of a photovoltaic device is generally expressed using eqn (8):[41,44–47]

$$\eta = \frac{J_{\mathrm{SC}} V_{\mathrm{OC}} \mathrm{FF}}{P_{\mathrm{in}}}, \quad (5)$$

where J_{SC}, V_{OC}, P_{in} and FF represent the short-circuit photocurrent density, open-circuit voltage, input power of incident sunlight and fill factor, respectively.

J_{SC} can be defined as:[41]

$$J_{\mathrm{SC}} = \int \mathrm{LHC}(\lambda)\phi_{\mathrm{inject}}\eta_{\mathrm{collect}}\mathrm{d}\lambda, \quad (6)$$

where, ϕ_{inject} and η_{collect} represent the measures of electron injection and electron collection, respectively.

The light harvesting capacity (LHC) and V_{OC} are two important parameters which help in calculating the efficiency of a dye. The LHC and V_{OC} can be obtained using eqn (7) and (8), respectively.[48]

$$\mathrm{LHC} = 1 - 10^{-f_{\mathrm{osc}}}, \quad (7)$$

$$V_{\mathrm{OC}} = E_{\mathrm{LUMO}} - E_{\mathrm{CB}}, \quad (8)$$

where f_{osc} is the oscillator strength corresponding to the wavelength of the absorption maxima and E_{LUMO} and E_{CB} correspond to the energies of the LUMO and CB of the semiconductor, respectively.

The thermodynamic driving force (ΔG^{inj}) for the transfer of an excited electron from the oxidised dye to the CB of the semiconductor is directly related to the excited state oxidation potential (ESOP), as given in eqn (9).[48]

$$\Delta G^{\mathrm{inj}} = \mathrm{ESOP} - E_{\mathrm{CB}}, \quad (9)$$

where ESOP is the energy difference between the ground state oxidation potential (GSOP) and first vertical excitation energy. The calculation of ESOP relative to the CB of TiO_2 serves as an important predictive tool for synthesizing new dyes, as well as for the interpretation of the photovoltaic data. For effective electron injection, the ESOP of the dye should lie above the CB of TiO_2. If it lies below the CB of TiO_2 (−4.0 eV), then unfavourable electron injection can take place and thereby we can predictively rule out the considered dye. The ESOP values can be evaluated using eqn (10).[48]

$$\mathrm{ESOP} = \mathrm{GSOP} + E_{\mathrm{g}}. \quad (10)$$

Here, GSOP is the energy difference between the neutral and oxidized charge species, and can be evaluated using eqn (11)[49]

$$\mathrm{GSOP} = E^{\circ}(\mathrm{M}^{\circ}) - E^{+}(\mathrm{M}^{\circ}), \quad (11)$$

and E_g represents the first excitation energy, *i.e.*, the energy corresponding to the lowest transition upon the absorption of light. The GSOP value of the dye should lie below the redox potential of the electrolyte I^{-}/I_3^{-} (−4.8 eV).[49] Several studies have revealed that the photovoltaic performance of DSSCs greatly depends on the driving force of the regeneration of the dye. Dye regeneration (ΔG^{reg}) is a process in which the oxidised dye after electron injection is regenerated by the redox electrolyte. ΔG^{reg} can be evaluated using eqn (12),[39]

$$\Delta G^{\mathrm{reg}} = E^{\mathrm{redox}}(I^{-}/I_3^{-}) - \mathrm{GSOP}. \quad (12)$$

The maximum absorption wavelength (λ_{max}) serves as an important parameter and can be defined as the wavelength along the absorption spectrum where a particular dye has its strongest photon absorption. When the absorption wavelength shifts toward a longer wavelength, it is called a red-shift and when it shifts toward a shorter wavelength, it is called a blue-shift. For larger conjugated systems, the absorption peak wavelengths tend to be shifted toward the longer wavelength region (*i.e.*, red-shift) and the absorption peaks tend to be larger.

In an organic system, the dipole moment (μ) is defined as the product of the magnitude of the charge and the distance between the centres of the positive and negative charges. It is a measure of the polarity of the organic dyes. A higher value of μ indicates the polar nature of that particular dye. The symbols μ_g and μ represent the dipole moment for the ground state and the excited state of organic dye molecules.

Another prominent parameter is the charge transfer rate (denoted by k_{CT}), which can be calculated through considering the π-stacking arrangement between two adjacent dyes. k_{CT} can be related to the reorganization energy (λ) using eqn (13).[43]

$$k_{\mathrm{CT}} = \left(\frac{\pi}{\lambda k_{\mathrm{B}} T}\right)^{1/2} \left(\frac{V^2}{\hbar}\right) \exp\left(-\frac{\lambda}{4 k_{\mathrm{B}} T}\right), \quad (13)$$

where T is the absolute temperature, k_B is the Boltzmann constant, $\hbar$ is the reduced Planck's constant and V is the electronic coupling matrix element between two adjacent dyes. The values of the electronic coupling matrix element for holes (V_+) and electrons (V_-) between two dye molecules are calculated as follows:[43]

$$V_{+(-)} = \frac{E_{H(L+1)} - E_{H-1(L)}}{2}, \quad (14)$$

where E_H, E_{H-1}, E_L and E_{L+1} represent the energies of the HOMO, HOMO−1, LUMO and LUMO+1, respectively, of the closed-shell configuration of the neutral state of the dyes. Another important parameter is the hopping mobility (μ_{hop}) which helps in quantifying the electron or hole transporting character of the dye molecule. We can evaluate the μ_{hop} values using eqn (15).[43]

$$\mu_{hop} = \frac{eD}{k_B T}, \quad (15)$$

where e denotes the electronic charge and D is the diffusion coefficient. In a one-dimensional charge transfer process, the value of D can be calculated using eqn (16).[43]

$$D = \frac{k_{CT} l^2}{2}, \quad (16)$$

where l represents the space distance between two interacting dye molecules.

4. Results and discussion

4.1 Dihedral angles

From the ground state calculations, we have evaluated the dihedral angles between the donor and the π-bridge (D–π), the π-bridge and the acceptor (π–A) and the acceptor and the anchoring group (A–A) of all of the dye-sensitizers. The obtained values of the dihedral angles are given in Table 1.

From Table 1, it is observed that among the unsubstituted dyes, the dyes TTF-DPP and TTF-QNX possess comparatively lower values of the dihedral angle between the donor and π-unit (D–π) than that of TTF-PTZ. Moreover, lower dihedral angle values are observed between the π-unit and the acceptor unit (π–A) for the dyes TTF-DPP and TTF-QNX compared to that of TTF-PTZ. We have also observed that the dihedral angle values between the acceptor unit and the anchoring group (A–A) are comparatively lower for the dyes TTF-DPP and TTF-QNX.

From Table 1, it is observed that the dihedral angles of the dyes are largely affected by the nature as well as the position of the substituents. In case of the TTF-PTZ group of dyes, higher values of the π–A angle are observed for TTF-PTZ-6′ (−55.80°) and TTF-PTZ-8′ (−62.52°) due to the attachment of the –NO_2 and –CF_3 groups at the acceptor part of the unsubstituted parent dye (*i.e.*, TTF-PTZ), respectively. In TTF-PTZ-6′, the observed π–A angle is high due to the electronegativity difference between the O-atom of the –NO_2 group and the S-atom of the thiophene ring. Moreover, for TTF-PTZ-8′, the π–A angle value is observed to be high due to repulsion between the electron-clouds of the H-atom of TTF and the S-atom of thiophene. It is also observed that the A–A angle in TTF-PTZ-6′ is comparatively higher (−27.42°) than those of the rest of the dyes so as to minimize the steric hindrance between the H-atom of acceptor moiety and the –CN group of the anchoring unit. In the case of the TTF-QNX group of dyes, the higher π–A distortion in TTF-QNX-6′ (32.04°) arises due to steric repulsion between the H-atom of the thiophene ring and the –NO_2 group attached to the acceptor part. However, for TTF-QNX-7′, it is observed that upon the attachment of the –F group at the acceptor part, the π–A angle is lowered compared to those of the other dyes. In the case of the TTF-DPP group of dyes, the π–A angle is found to be lower (∼1–2°) upon the inclusion of the electron donating groups at the donor part, whereas it seems to be higher (18–19°) for the electron withdrawing groups substituted at the acceptor part. This is because of the larger size of the acceptor moiety, which sterically hinders the thiophene ring. Hence, the TTF-DPP and TTF-QNX groups of dyes possess a comparatively planar structure among all of the designed dyes.

4.2 Frontier molecular orbital analysis

We have calculated the energies of the HOMOs and LUMOs of all of the dye systems and their respective values are given in Table 2, along with the Δ_{H-L} values.

From Table 2, it is observed that among the three unsubstituted parent dyes, *viz.*, TTF-PTZ, TTF-DPP and TTF-QNX, the lowest Δ_{H-L} value is observed for TTF-DPP (1.53 eV), followed by TTF-PTZ (1.70 eV), while it is the highest for TTF-QNX (2.09 eV). The energy band-gap values for the TTF-DPP and TTF-PTZ groups of dyes are nearly the same due to their similar HOMO and LUMO energy levels. It is also observed that for all of the designed dyes, the HOMOs are less affected upon the inclusion of various substituents. However, the LUMOs are markedly

Table 1 The observed dihedral angles between different parts of the dye systems

Dye	D–π (°)	π–A (°)	A–A (°)	Dye	D–π (°)	π–A (°)	A–A (°)	Dye	D–π (°)	π–A (°)	A–A (°)
TTF-PTZ	23.59	−38.09	−18.62	TTF-DPP	−18.36	1.91	−1.56	TTF-QNX	22.45	−24.16	0.13
TTF-PTZ-1	−23.33	−37.94	−18.39	TTF-DPP-1	−18.17	1.80	−1.53	TTF-QNX-1	22.86	−23.22	0.12
TTF-PTZ-2	22.93	−38.41	−19.33	TTF-DPP-2	−17.80	2.28	−1.55	TTF-QNX-2	23.07	−23.20	0.07
TTF-PTZ-3	23.10	−38.08	−18.79	TTF-DPP-3	−18.68	2.03	−1.57	TTF-QNX-3	23.09	−23.26	0.10
TTF-PTZ-4	−19.42	−37.70	−18.47	TTF-DPP-4	−18.05	2.01	−1.48	TTF-QNX-4	−21.96	−23.39	0.10
TTF-PTZ-5	23.74	−38.22	−18.50	TTF-DPP-5	−18.71	1.90	−1.52	TTF-QNX-5	22.98	−23.76	0.11
TTF-PTZ-6′	27.03	−55.80	−27.42	TTF-DPP-6′	−19.23	18.49	−2.16	TTF-QNX-6′	20.48	32.04	0.08
TTF-PTZ-7′	23.33	−40.41	−15.75	TTF-DPP-7′	17.86	−6.88	−1.03	TTF-QNX-7′	22.34	−15.23	0.14
TTF-PTZ-8′	25.22	−62.52	25.70	TTF-DPP-8′	17.45	19.90	−3.45	TTF-QNX-8′	23.87	−42.76	0.11

Table 2 Energies of the frontier molecular orbitals of the dye systems and their corresponding Δ_{H-L} values

Dye	HOMO (eV)	LUMO (eV)	Δ_{H-L} (eV)	Dye	HOMO (eV)	LUMO (eV)	Δ_{H-L} (eV)	Dye	HOMO (eV)	LUMO (eV)	Δ_{H-L} (eV)
TTF-PTZ	−4.97	−3.27	1.70	TTF-DPP	−5.01	−3.48	1.53	TTF-QNX	−4.76	−2.67	2.09
TTF-PTZ-1	−4.86	−3.24	1.62	TTF-DPP-1	−4.91	−3.45	1.46	TTF-QNX-1	−4.66	−2.65	2.01
TTF-PTZ-2	−4.96	−3.25	1.71	TTF-DPP-2	−4.97	−3.47	1.50	TTF-QNX-2	−4.82	−2.68	2.14
TTF-PTZ-3	−4.78	−3.23	1.55	TTF-DPP-3	−4.83	−3.44	1.39	TTF-QNX-3	−4.61	−2.64	1.97
TTF-PTZ-4	−4.74	−3.24	1.50	TTF-DPP-4	−4.85	−3.62	1.23	TTF-QNX-4	−4.56	−2.65	1.91
TTF-PTZ-5	−4.91	−3.27	1.64	TTF-DPP-5	−5.01	−3.50	1.51	TTF-QNX-5	−4.72	−2.68	2.04
TTF-PTZ-6′	−4.95	−3.62	1.33	TTF-DPP-6′	−5.21	−3.98	1.23	TTF-QNX-6′	−4.89	−3.37	1.52
TTF-PTZ-7′	−4.94	−3.40	1.54	TTF-DPP-7′	−5.12	−3.74	1.38	TTF-QNX-7′	−4.79	−2.81	1.98
TTF-PTZ-8′	−4.91	−3.44	1.47	TTF-DPP-8′	−5.09	−3.72	1.37	TTF-QNX-8′	−4.82	−3.07	1.75

affected by the various substituents. In the case of the TTF-QNX group of dyes, the LUMO energy levels are increased, which in turn leads to the observed highest Δ_{H-L} values. A lower fundamental gap facilitates the better excitation of the organic dyes. From this point of view, the TTF-DPP group of dyes can be considered to be potential candidates for DSSCs. However, the most efficient of the respective dyes cannot be decided for this purpose based on a single parameter. We present the frontier molecular orbital diagrams of the three parent dye systems in Fig. 2. From Fig. 2, it is clear that the HOMOs are delocalized over the donor part, with some contribution on the π-bridge unit. On the other hand, the LUMOs are delocalized over the acceptor part, with some contribution on the π-bridge unit and the anchoring group.

From Table 2, it is observed that attachment of the $-NH_2$ group at the donor part lowers the Δ_{H-L} values of all three dye systems. This is probably due to the extension in conjugation of the donor TTF moiety, as well as the strong electron donating nature of the $-NH_2$ group. Moreover, attachment of the $-NO_2$ and $-CF_3$ groups at the acceptor part results in lowering of the Δ_{H-L} values for all three dye systems. This can be attributed to the highly electron withdrawing nature of the $-NO_2$ and $-CF_3$ groups. It is also observed from Table 2 that the $-NH_2$, $-NO_2$ and $-CF_3$ substituted dyes show relatively lower Δ_{H-L} values compared to those of the other substituted dyes. Among all of the designed dyes, TTF-DPP-4 and TTF-DPP-6′ exhibit the lowest values of Δ_{H-L} (1.23 eV for both). This lowering of the band gap is solely due to the extended delocalization of the electron cloud and the strongly electron donating/withdrawing nature of the $-NH_2$ and $-NO_2$ groups, respectively. We present the frontier molecular orbitals of the $-NH_2$, $-NO_2$ and $-CF_3$ substituted TTF-PTZ, TTF-DPP and TTF-QNX dyes in Fig. 3.

From Fig. 3, it is observed that the HOMOs are delocalized over the donor part in the dyes TTF-PTZ-4, TTF-PTZ-6′, TTF-PTZ-8′, TTF-DPP-4, TTF-DPP-6′, TTF-QNX-6′ and TTF-QNX-8′. On the other hand, the LUMOs are delocalized over the π-bridging unit and acceptor part and extended to the anchoring group in these dyes. However, in case of TTF-QNX-4, it is observed that the HOMO is delocalized over the π-bridging unit and acceptor part and extended to the anchoring group. On the other hand, the LUMO is delocalized over the acceptor part and extended to the anchoring group in this dye. Moreover, in the case of TTF-DPP-8′, the HOMO is delocalized over the π-conjugated molecular backbone, while the LUMO is delocalized over the donor part and the anchoring group.

4.3 Density of states of the dyes

The density of states (DOS) can be defined as the number of different states available for electrons present in a system in

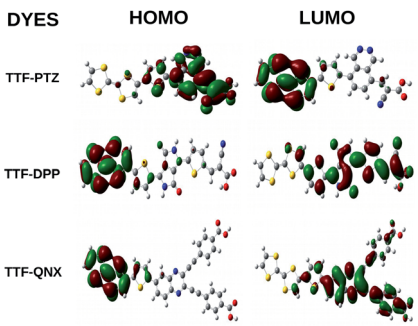

Fig. 2 Plot of the frontier molecular orbitals of the three parent dyes.

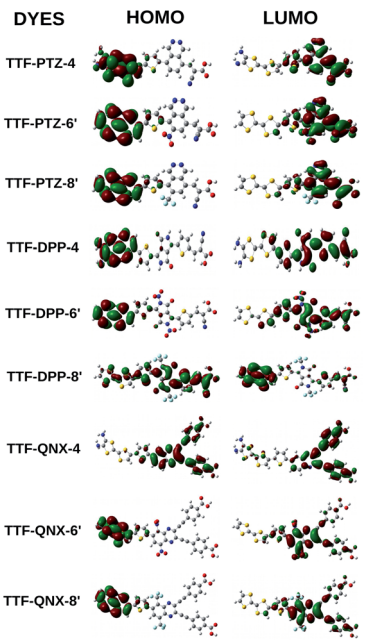

Fig. 3 Plot of the frontier molecular orbitals of the $-NH_2$, $-NO_2$ and $-CF_3$ substituted TTF-PTZ, TTF-DPP and TTF-QNX dyes.

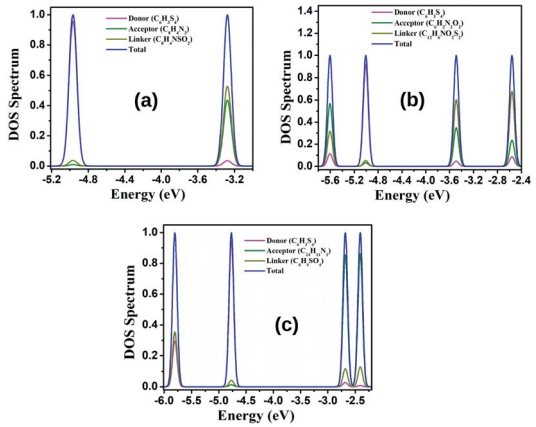

Fig. 4 PDOS spectra of the unsubstituted parent dyes (a) TTF-PTZ, (b) TTF-DPP and (c) TTF-QNX.

a particular energy level. The partial density of states (PDOS) signifies the relative contribution of a particular orbital or atom to the total DOS.[50–53] We have calculated the PDOS of our designed dyes to make a comparative study of their electronic properties with the frontier molecular orbitals (FMOs). The PDOSs of the designed dyes have been calculated and their respective spectral data are reported in Table S3 (in the ESI†). From this table, it is observed that the donor unit offers the maximum contribution to the HOMOs, while the acceptor unit contributes minimally to the HOMOs. Moreover, for the TTF-PTZ and TTF-DPP groups of dyes, the bridging unit offers the maximum contribution to the LUMOs, while the donor unit offers the minimum contribution to the LUMOs. However, for the TTF-QNX group of dyes, it is observed that the acceptor part offers the maximum contribution to the LUMOs, while the donor part contributes minimally. In TTF-PTZ-6′, where the acceptor unit is substituted with the $-NO_2$ group, a dominant contribution of the acceptor unit to the LUMO is observed. Thus, it can be concluded that the attachment of electron donating groups at the donor unit increases the contribution of the donor unit to the HOMO energy level. Therefore, these observed facts reveal that the PDOS spectra provide a clear view of the nature of the HOMO and LUMO energy levels. The PDOS spectra of the unsubstituted parent dyes are provided in Fig. 4 and the same spectra for the other dyes are provided in Fig. S3 (in the ESI†).

4.4 Oxidation potential of the dyes

It is already known that for effective electron injection and dye regeneration processes, the frontier orbitals of the dye and semiconductor should be appropriately aligned. To examine these processes, we have calculated the GSOP and ESOP values for the designed dyes by performing TD-DFT calculations on the optimized geometries. Moreover, to gain more insight into the charge transfer process, we have also calculated the ΔG^{reg} and ΔG^{inj} values. The values of ΔG^{inj}, ESOP, GSOP and ΔG^{reg} can be calculated using eqn (9)–(12), respectively. The calculated values of GSOP, ESOP, ΔG^{reg} and ΔG^{inj} are given in Table 3. We also present the plots of the band alignments of the TTF-PTZ, TTF-DPP and TTF-QNX groups of dyes, with respect to the CB of TiO_2 and the redox potential of I^-/I_3^-, in Fig. 5.

Table 3 Calculated values of GSOP, ESOP, ΔG^{reg} and ΔG^{inj} of the studied dye systems

Dye	GSOP (eV)	ESOP (eV)	ΔG^{reg} (eV)	ΔG^{inj} (eV)
TTF-PTZ	−6.18	−3.37	1.38	0.63
TTF-PTZ-1	−6.02	−3.24	1.22	0.76
TTF-PTZ-2	−6.21	−3.37	1.44	0.63
TTF-PTZ-3	−5.86	−3.04	1.06	0.96
TTF-PTZ-4	−5.74	−2.95	0.94	1.05
TTF-PTZ-5	−6.12	−3.30	1.32	0.70
TTF-PTZ-6′	−6.18	−3.52	1.38	0.48
TTF-PTZ-7′	−6.16	−3.44	1.36	0.56
TTF-PTZ-8′	−6.16	−3.29	1.36	0.71
TTF-DPP	−6.05	−3.90	1.25	0.1
TTF-DPP-1	−5.92	−4.01	1.12	−0.01
TTF-DPP-2	−5.89	−3.74	1.09	0.26
TTF-DPP-3	−5.83	−3.68	1.03	0.32
TTF-DPP-4	−5.68	−3.53	0.88	0.47
TTF-DPP-5	−6.03	−3.87	1.23	0.13
TTF-DPP-6′	−6.29	−4.27	1.49	−0.27
TTF-DPP-7′	−6.20	−4.08	1.40	−0.08
TTF-DPP-8′	−6.17	−4.01	1.37	−0.01
TTF-QNX	−5.92	−2.87	1.12	1.13
TTF-QNX-1	−5.79	−2.76	0.99	1.24
TTF-QNX-2	−5.83	−2.74	1.03	1.26
TTF-QNX-3	−5.66	−2.57	0.86	1.43
TTF-QNX-4	−5.54	−2.50	0.74	1.5
TTF-QNX-5	−5.88	−2.80	1.08	1.2
TTF-QNX-6′	−6.08	−3.39	1.28	0.61
TTF-QNX-7′	−5.95	−2.98	1.15	1.02
TTF-QNX-8′	−6.01	−3.12	1.21	0.88

From Table 3 and Fig. 5, it is observed that for the TTF-PTZ and TTF-QNX groups of dyes, the GSOP values lie below the redox potential of the I^-/I_3^- electrolyte couple and the ESOP values lie above the conduction band of TiO_2. Moreover, for the TTF-DPP group of dyes, the GSOP values lie below the redox potential of the I^-/I_3^- electrolyte couple and the ESOP values lie above the conduction band of the TiO_2 (except TTF-DPP-1, TTF-DPP-6′, TTF-DPP-7′ and TTF-DPP-8′). This indicates that all of the designed dyes have the potential to serve as candidates for the fabrication of DSSCs.

It is noteworthy to mention that higher ΔG^{inj} values of the dyes indicate higher efficiency towards electron injection. Moreover, for efficient dye regeneration, the ΔG^{reg} values must lie within a threshold limit of 0.2–0.3 eV.[41] From Table 3, it is observed that the ΔG^{inj} values are comparatively higher for the TTF-QNX groups of dyes than the other groups of dyes. However, the ΔG^{reg} values for the dyes TTF-PTZ-4, TTF-DPP-4, TTF-QNX-1, TTF-QNX-3 and TTF-QNX-4 are close to the threshold values compared to the other designed dyes. In this regard, the above mentioned groups of dyes will be more efficient toward dye regeneration.

The electron injection and the dye regeneration processes can also be justified in terms of the electron affinity (EA) and ionization potential (IP) of the dyes. It has been already reported that a low IP facilitates the removal of electrons, which in turn

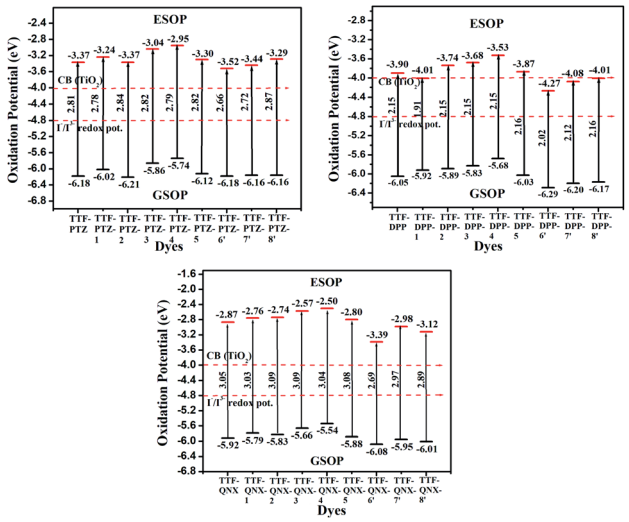

Fig. 5 Plots of the band alignments of the TTF-PTZ, TTF-DPP and TTF-QNX groups of dyes with respect to CB of TiO_2 and redox potential of I^-/I_3^-.

facilitates the generation of holes. In addition, the EA value of the dye molecule explains the recombination between the injected electron and the oxidized dye species. A low EA value ensures the easy removal of electrons from the conduction band.[41] The calculated values of IP and EA for the studied dyes (using eqn (1) and (2), respectively) are given in Table 4.

For efficient electron transfer from the dye to the semiconducting surface, low IP and EA values are preferable for a dye-sensitizer. From Table 4, it is evident that most of the substituted variants of the dyes exhibit lower IP values than those of their parent dyes. Hence, our designed dyes meet the requirements for becoming suitable dye-sensitizers. Furthermore, it is observed that the TTF-QNX group of dyes possesses comparatively lower values of IP and EA than those of the other groups of dyes. This indicates that the TTF-QNX group of dyes may serve as better candidates for the construction of DSSCs.

4.5 Absorption properties of the dyes

For better understanding the absorption properties of the designed dyes, the excitation properties have been extracted for 30 excited states and the dominant electronic transitions are given in Table 5. We also provide the values of the excitation energies (E_g), maximum absorption wavelengths (λ_{max}), oscillator strengths (f_{osc}), light harvesting capacities (LHC), open-circuit voltages (V_{OC}) and dipole moments (μ) *etc.* in Table 5.

From Table 5, it is observed that TTF-DPP group of dyes possesses comparatively higher f_{osc} values and μ values compared to those of the other groups of dyes. The higher μ values indicate that the studied dyes are polar in nature. Among the unsubstituted parent dyes, TTF-DPP possesses the highest value of λ_{max} compared to those of the other two dyes. This is consistent with the observed Δ_{H-L} values for the unsubstituted parent dyes, which exhibit the following trend: TTF-DPP (1.51 eV) < TTF-PTZ (1.69 eV) < TTF-QNX (2.08 eV). In addition, the λ_{max} values for the TTF-PTZ and TTF-QNX groups of dyes correspond to H → L transitions, with configurations ranging from 60–75% and 30–71%, respectively. On the other hand, in case of the TTF-DPP group of dyes, the λ_{max} values for those with electron donating substituents correspond to the transition H−1 → L, while for those with electron withdrawing substituents, the λ_{max} values correspond to the H → L transition with configurations ranging from 45–70%. Among the TTF-PTZ and TTF-QNX groups of dyes, the λ_{max} values are observed to be maximum for TTF-PTZ-6′ and TTF-QNX-6′, where the $-NO_2$ group is substituted at the acceptor part. Due to the presence of the $-NO_2$ group at the acceptor part, the electron density increases, which results in the maximum red-shift of the respective dyes. Moreover, in case of the TTF-DPP group of dyes, the maximum λ_{max} value is exceptionally observed for TTF-DPP-1. The presence of the $-CH_3$ group at the donor part increases the electron density of TTF-DPP-1 and therefore results in the maximum red-shift. The corresponding spectra are provided in Fig. 6.

From eqn (6), it can be inferred that a high LHC value will lead to a high J_{SC} value. From the calculated values of LHC (as given in Table 5), it is observed that the LHC values for the TTF-DPP and TTF-QNX groups of dyes are comparatively higher than those of the TTF-PTZ group of dyes. It is also observed that among all the studied dyes, TTF-QNX-2 possesses the maximum LHC value and TTF-PTZ-6′ possesses the minimum value of LHC. Hence, taking into account the LHC values, it can be said that the J_{SC} values are slightly higher for the TTF-DPP and TTF-QNX groups of dyes compared to those of the TTF-PTZ group of dyes.

Eqn (5) manifests that a high value of the open-circuit voltage (V_{OC}) is needed to achieve the high energy conversion

Table 4 Calculated values of the IP and EA of the studied dye systems

Compound	IP (eV)	EA (eV)	Compound	IP (eV)	EA (eV)	Compound	IP (eV)	EA (eV)
TTF-PTZ	6.18	2.19	TTF-DPP	6.05	2.52	TTF-QNX	5.92	1.75
TTF-PTZ-1	6.02	2.16	TTF-DPP-1	5.92	2.49	TTF-QNX-1	5.79	1.73
TTF-PTZ-2	6.21	2.28	TTF-DPP-2	5.89	2.52	TTF-QNX-2	5.83	1.76
TTF-PTZ-3	5.86	2.15	TTF-DPP-3	5.83	2.49	TTF-QNX-3	5.66	1.72
TTF-PTZ-4	5.74	2.15	TTF-DPP-4	5.68	2.48	TTF-QNX-4	5.54	1.73
TTF-PTZ-5	6.12	2.19	TTF-DPP-5	6.03	2.54	TTF-QNX-5	5.88	1.76
TTF-PTZ-6′	6.18	2.54	TTF-DPP-6′	6.29	3.06	TTF-QNX-6′	6.08	2.47
TTF-PTZ-7′	6.16	2.30	TTF-DPP-7′	6.20	2.79	TTF-QNX-7′	5.95	1.88
TTF-PTZ-8′	6.16	2.34	TTF-DPP-8′	6.17	2.79	TTF-QNX-8′	6.01	2.14

Table 5 E_g, λ_{max}, f_{osc}, electronic transitions, LHC, μ and V_{OC} of the studied dye systems

Dye	E_g (eV)	λ_{max} (nm)	f_{osc}	Transition	LHC	μ (Debye)	V_{OC}
TTF-PTZ	2.81	440	0.71	H → L (67%)	0.806	4.89	0.73
TTF-PTZ-1	2.78	444	0.70	H → L (68%)	0.801	6.06	0.76
TTF-PTZ-2	2.84	435	0.83	H → L (65%)	0.852	7.03	0.75
TTF-PTZ-3	2.82	439	0.74	H → L (64%)	0.819	7.59	0.77
TTF-PTZ-4	2.79	444	0.61	H → L (65%)	0.758	7.92	0.76
TTF-PTZ-5	2.82	438	0.69	H → L (61%)	0.799	5.68	0.73
TTF-PTZ-6′	2.66	465	0.32	H → L (78%)	0.522	4.45	0.38
TTF-PTZ-7′	2.72	454	0.67	H → L (71%)	0.787	4.31	0.60
TTF-PTZ-8′	2.87	430	0.39	H → L (75%)	0.594	4.86	0.56
TTF-DPP	2.15	574	1.38	H−1 → L (51%)	0.958	12.03	0.52
TTF-DPP-1	1.91	647	1.52	H−1 → L (52%)	0.969	13.41	0.55
TTF-DPP-2	2.15	574	1.44	H−1 → L (48%)	0.964	12.88	0.53
TTF-DPP-3	2.15	575	1.42	H−1 → L (55%)	0.962	14.29	0.56
TTF-DPP-4	2.15	576	1.39	H−1 → L (60%)	0.960	14.44	0.38
TTF-DPP-5	2.16	571	1.39	H−1 → L (55%)	0.959	11.55	0.50
TTF-DPP-6′	2.02	611	1.09	H → L (69%)	0.919	13.24	0.02
TTF-DPP-7′	2.12	583	1.33	H → L (54%)	0.953	12.06	0.26
TTF-DPP-8′	2.16	571	1.28	H → L (53%)	0.947	12.31	0.29
TTF-QNX	3.05	406	1.40	H → L (42%)	0.961	3.18	1.33
TTF-QNX-1	3.03	408	1.39	H → L (42%)	0.959	3.95	1.35
TTF-QNX-2	3.09	400	1.74	H → L (42%)	0.981	2.88	1.32
TTF-QNX-3	3.09	400	1.20	H → L (31%)	0.938	4.78	1.36
TTF-QNX-4	3.04	406	1.16	H → L (36%)	0.931	3.34	1.35
TTF-QNX-5	3.08	402	1.47	H → L (41%)	0.966	3.58	1.32
TTF-QNX-6′	2.69	459	0.71	H → L (71%)	0.809	0.91	0.63
TTF-QNX-7′	2.97	417	1.33	H → L (47%)	0.953	2.45	1.19
TTF-QNX-8′	2.89	428	1.02	H → L (62%)	0.904	2.91	0.93

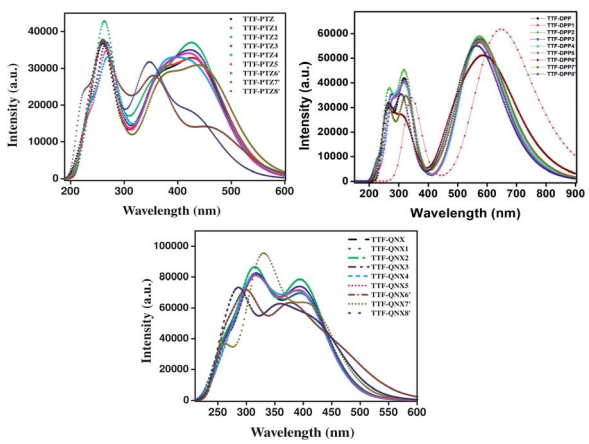

Fig. 6 UV–visible spectra of TTF-PTZ, TTF-DPP, TTF-QNX and their derivatives.

efficiency (η) of a photovoltaic device. In this regard, we have calculated the V_{OC} for all of the studied dyes and they are given in Table 5. From Table 5, it is observed that the TTF-QNX group of dyes shows comparatively higher values of V_{OC} than those of the other groups of dyes. This observed fact will lead to a higher efficiency of energy conversion in these dyes.

To have a better understanding of charge transportation in the designed dyes, we have calculated the reorganization energies (λ) and they are given in Table 6. There are two dominant factors, *i.e.*, the structural effects and the electronic effects, which help in determining the λ values for both holes (λ_+) and electrons (λ_-).[40] The λ value (λ_+ or λ_-) needs to be small for effective charge transportation. The lower the λ_- value, the higher the electron transporting capacity of the dye will be. Conversely, a lower λ_+ value reflects the hole transporting nature of the dyes.

From Table 6, it is observed that in case of the TTF-PTZ group of dyes, the λ_+ values for the dyes TTF-PTZ, TTF-PTZ-2, TTF-PTZ-5, TTF-PTZ-7′ and TTF-PTZ-8′ are lesser than the λ_- values. This in turn implies a facile hole transportation in the these dyes. However, for the dyes TTF-PTZ-1, TTF-PTZ-3, TTF-PTZ-4 and TTF-PTZ-6′, λ_- values are smaller than the λ_+ values which indicates the greater ease of electron transportation in these dyes. Besides, in case of the TTF-DPP groups of dyes, a relatively smaller value of λ_+ is observed for the dyes TTF-DPP, TTF-DPP-1 and TTF-DPP-8′ indicating facile hole transportation. However, the electron transportation capacity will be higher for the dyes TTF-DPP-2, TTF-DPP-3, TTF-DPP-4, TTF-DPP-5, TTF-DPP-6′ and TTF-DPP-7′. Moreover, it is observed that in case of the TTF-QNX groups of dyes, all possess a smaller value of λ_- which clearly indicates the dominant electron transportation capacity.

We have also calculated the total reorganization energy (λ_{tot}) values and the same are reported in Table 6. λ_{tot} is simply the sum of the values of λ_+ and λ_-. For efficient electron–hole separation, the λ_{tot} values of the dyes should be small, which results in the mitigation of the recombination processes.[41]

Table 6 Calculated values of the reorganization energies of the studied dyes

Dye	λ_+ (eV)	λ_- (eV)	λ_{tot} (eV)	Dye	λ_+ (eV)	λ_- (eV)	λ_{tot} (eV)	Dye	λ_+ (eV)	λ_- (eV)	λ_{tot} (eV)
TTF-PTZ	0.342	0.361	0.703	TTF-DPP	0.247	0.277	0.524	TTF-QNX	0.299	0.220	0.519
TTF-PTZ-1	0.367	0.361	0.728	TTF-DPP-1	0.269	0.277	0.546	TTF-QNX-1	0.323	0.220	0.543
TTF-PTZ-2	0.413	0.422	0.835	TTF-DPP-2	0.307	0.280	0.587	TTF-QNX-2	0.345	0.220	0.565
TTF-PTZ-3	0.424	0.364	0.788	TTF-DPP-3	0.329	0.283	0.612	TTF-QNX-3	0.337	0.215	0.552
TTF-PTZ-4	0.459	0.373	0.832	TTF-DPP-4	0.326	0.285	0.611	TTF-QNX-4	0.392	0.228	0.620
TTF-PTZ-5	0.362	0.367	0.729	TTF-DPP-5	0.296	0.283	0.579	TTF-QNX-5	0.302	0.220	0.522
TTF-PTZ-6′	0.383	0.381	0.764	TTF-DPP-6′	0.307	0.261	0.568	TTF-QNX-6′	0.335	0.332	0.667
TTF-PTZ-7′	0.342	0.351	0.693	TTF-DPP-7′	0.274	0.269	0.543	TTF-QNX-7′	0.305	0.231	0.536
TTF-PTZ-8′	0.372	0.416	0.788	TTF-DPP-8′	0.282	0.296	0.578	TTF-QNX-8′	0.324	0.239	0.563

From Table 6, it is observed that the TTF-DPP and TTF-QNX groups of dyes possess low values of λ_{tot} compared to those of the TTF-PTZ group of dyes. This reveals the better electron–hole separation efficiency in the TTF-DPP and TTF-QNX groups of dyes and they may have slower recombination processes compared to those of the TTF-PTZ groups of dyes.

To gauge the electronic coupling matrix element (V), we have considered the π-stacking arrangement of the two adjacent dyes. The representative structures of two stacked dyes are presented in Fig. S4 (in the ESI†) and the calculated V values (using eqn (14)) are given in Table 7. Using the V values, we have calculated another parameter *i.e.*, the charge transfer rates for holes (k_{CT}^{+}) and electrons (k_{CT}^{-}) (using eqn (13)) and given in Table 7.

From Table 7, it is evident that the k_{CT}^{-} values are higher than the k_{CT}^{+} values for almost all of the studied dyes except TTF-PTZ-2, TTF-PTZ-5, TTF-DPP-4, TTF-DPP-8′ and TTF-QNX-5. This implies that the dyes with higher k_{CT}^{-} values will act as electron-transporting materials and those with higher k_{CT}^{+} values will act as hole-transporting materials. Another important parameter is the hopping mobility (μ_{hop}), which helps in determining the conducting capacity of the organic dyes. A high μ_{hop} value signifies higher electronic coupling between the adjacent dyes, which in turn indicates the better conducting capacity of the organic dyes. The calculated μ_{hop} values for holes and electrons are reported in Table 7. From this table, it is observed that among all the studied dyes, TTF-QNX-5 possesses the highest value of μ_{hop}^{+}, whereas TTF-DPP-3 possesses the highest value of μ_{hop}^{-}. These values are in accordance with the observed values of k_{CT}^{+} and k_{CT}^{-} for these dyes, respectively. Hence, our designed dyes may act as potential candidates for the fabrication of optoelectronic devices.

Table 7 V, k_{CT} and μ_{hop} values of the studied dyes

Dye	V_+ (eV)	V_- (eV)	$k_{CT}^{+} \times 10^{13}$ (s^{-1})	$k_{CT}^{-} \times 10^{13}$ (s^{-1})	l (A°)	μ_{hop}^{+} ($cm^2\ V^{-1}\ s^{-1}$)	μ_{hop}^{-} ($cm^2\ V^{-1}\ s^{-1}$)
TTF-PTZ	0.059	0.170	0.364	2.453	3.00	0.063	0.426
TTF-PTZ-1	0.034	0.168	2.701	14.263	3.58	0.669	3.528
TTF-PTZ-2	0.201	0.195	9.649	8.489	3.66	2.499	2.199
TTF-PTZ-3	0.186	0.188	7.923	15.441	3.03	1.407	2.741
TTF-PTZ-4	0.181	0.190	5.282	14.131	3.01	0.925	2.476
TTF-PTZ-5	0.269	0.179	22.587	14.223	3.03	4.010	2.525
TTF-PTZ-6′	0.054	0.236	3.598	16.073	3.52	0.862	3.851
TTF-PTZ-7′	0.134	0.405	14.046	38.412	3.00	2.445	6.686
TTF-PTZ-8′	0.044	0.126	3.308	5.854	3.63	0.843	1.491
TTF-DPP	0.025	0.260	7.727	56.780	3.51	1.841	13.529
TTF-DPP-1	0.017	0.132	4.070	28.827	2.92	0.671	4.753
TTF-DPP-2	0.213	0.191	33.058	40.301	3.44	7.565	9.223
TTF-DPP-3	0.116	0.080	14.058	112.839	3.51	3.349	26.886
TTF-DPP-4	0.251	0.147	31.458	29.293	2.91	5.152	4.794
TTF-DPP-5	0.020	0.156	4.788	31.805	2.89	0.773	5.137
TTF-DPP-6′	0.055	0.167	8.536	43.859	3.17	1.659	8.524
TTF-DPP-7′	0.031	0.368	7.007	88.113	3.59	1.746	21.963
TTF-DPP-8′	0.158	0.165	32.583	29.007	3.58	8.076	7.190
TTF-QNX	0.052	0.108	8.835	45.928	3.57	2.182	11.321
TTF-QNX-1	0.011	0.058	1.426	24.665	2.88	0.228	3.956
TTF-QNX-2	0.149	0.073	15.701	30.188	3.59	3.913	7.524
TTF-QNX-3	0.085	0.067	9.420	30.249	3.55	2.296	7.373
TTF-QNX-4	0.250	0.099	15.092	38.276	2.92	2.488	6.311
TTF-QNX-5	0.262	0.053	43.029	22.538	3.54	10.428	5.462
TTF-QNX-6′	0.075	0.075	8.499	8.789	3.24	1.725	1.784
TTF-QNX-7′	0.205	0.123	32.544	45.895	2.89	5.256	7.407
TTF-QNX-8′	0.239	0.196	30.633	66.546	3.59	7.635	16.587

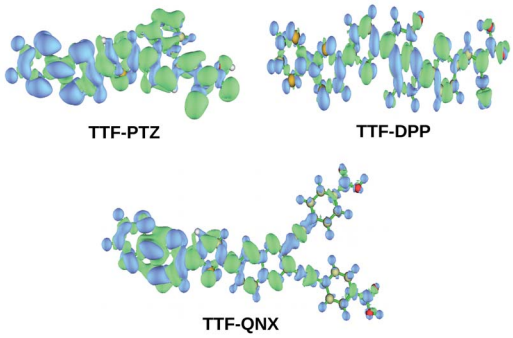

Fig. 7 Electron density difference (EDD) maps for the unsubstituted parent dyes.

4.6 Electron density difference (EDD) maps of the dyes

To illustrate the distribution of electron density in the designed dyes that occurs during the $S_0 \rightarrow S_1$ transition, we have carried out an efficient analysis of the electronic structures of the designed dyes and portrayed their electron density difference (EDD) maps with the help of Multiwfn program package.[54–56] We provide the EDD map for the unsubstituted parent dyes in Fig. 7. For the rest of the dyes, we provide the EDD maps in Fig. S5 (in the ESI†). In Fig. 7 and S5,† green and blue regions correspond to the increase and decrease in electron density, respectively, due to the excitation of electrons during the $S_0 \rightarrow S_1$ transition.

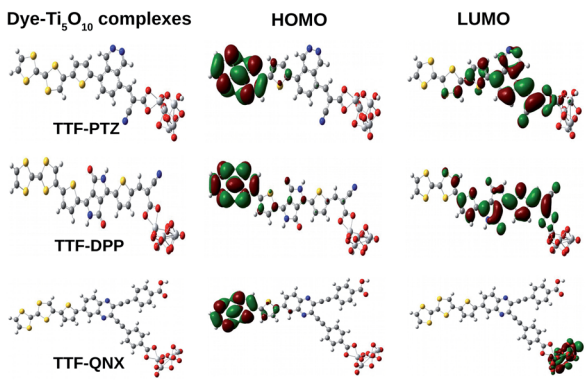

Fig. 8 Optimized geometries of the unsubstituted dye–Ti_5O_{10} clusters, along with their frontier molecular orbitals.

From Fig. 7, it is observed that the acceptor unit exhibits the maximum electron density whereas the donor unit exhibits the minimum electron density. Hence, it can be inferred that during the $S_0 \rightarrow S_1$ transition, charge transfer occurs from the donor unit to the acceptor unit for all of the designed dyes.

4.7 Adsorption on TiO_2 surfaces

In order to simulate the performance of a more naturalistic solar cell device, it is very important to investigate the optical properties of the designed dyes. We have adopted a Ti_5O_{10} cluster to represent the TiO_2 semiconductor surface for this purpose. Here, we have used cyanoacrylic acid and bidentate carboxylate groups as the anchoring groups to enable the adsorption of the dye-sensitizers to the semiconducting surface. These anchoring groups have been proven to be the most ideal anchoring mode in DSSCs.[41] We present the optimized structures of the three unsubstituted dye–Ti_5O_{10} clusters, *viz.*, TTF-DPP–Ti_5O_{10}, TTF-PTZ–Ti_5O_{10}, TTF-QNX–Ti_5O_{10}, along with their HOMOs and LUMOs, in Fig. 8.

From Fig. 8, it can be observed that for the dye clusters TTF-DPP–Ti_5O_{10} and TTF-PTZ–Ti_5O_{10}, the HOMOs are primarily delocalized over the donor part with contributions from the π-bridging units of the dyes. On the other hand, the LUMOs are primarily delocalized over the acceptor part with contributions from the π-bridging unit and the donor part. However, for the dye cluster TTF-QNX–Ti_5O_{10}, the HOMO is primarily delocalized over the donor part with contribution from the π-bridging unit and the LUMO is primarily delocalized over the Ti_5O_{10} semiconducting surface.

We have calculated the Ti–O bond lengths of the studied dyes and they are given in Table 8. A representation of the Ti–O bond length in the representative TTF-PTZ–Ti_5O_{10} cluster is presented in Fig. 9.

From Table 8, it can be observed that the Ti–O bond lengths of all of the studied dyes are in the range of 2.011–2.055 Å. These values are consistent with the theoretically reported Ti–O bond lengths (2.03–2.24 Å) for various dye–TiO_2 clusters.[41,57] Therefore, this suggests that all of the designed dyes undergo chemisorption on the TiO_2 surface.

We have also calculated the Δ_{H-L} values and the ground state dipole moments (μ_g) of the studied dye–Ti_5O_{10} clusters and they are reported in Table 9.

From a comparison of Table 2 and Table 9, it is observed that the Δ_{H-L} values of the isolated dyes are larger than those of the

Table 8 Ti–O bond lengths of the dye–Ti_5O_{10} clusters

Dye–Ti_5O_{10}	Ti–O_a (Å)	Ti–O_b (Å)	Dye–Ti_5O_{10}	Ti–O_a (Å)	Ti–O_b (Å)	Dye–Ti_5O_{10}	Ti–O_a (Å)	Ti–O_b (Å)
TTF-PTZ–Ti_5O_{10}	2.031	2.045	TTF-DPP–Ti_5O_{10}	2.013	2.046	TTF-QNX–Ti_5O_{10}	2.021	2.031
TTF-PTZ-1–Ti_5O_{10}	2.029	2.044	TTF-DPP-1–Ti_5O_{10}	2.012	2.045	TTF-QNX-1–Ti_5O_{10}	2.021	2.030
TTF-PTZ-2–Ti_5O_{10}	2.031	2.046	TTF-DPP-2–Ti_5O_{10}	2.013	2.047	TTF-QNX-2–Ti_5O_{10}	2.022	2.031
TTF-PTZ-3–Ti_5O_{10}	2.029	2.043	TTF-DPP-3–Ti_5O_{10}	2.012	2.046	TTF-QNX-3–Ti_5O_{10}	2.022	2.031
TTF-PTZ-4–Ti_5O_{10}	2.029	2.044	TTF-DPP-4–Ti_5O_{10}	2.011	2.045	TTF-QNX-4–Ti_5O_{10}	2.021	2.031
TTF-PTZ-5–Ti_5O_{10}	2.031	2.046	TTF-DPP-5–Ti_5O_{10}	2.012	2.046	TTF-QNX-5–Ti_5O_{10}	2.022	2.031
TTF-PTZ-6′–Ti_5O_{10}	2.038	2.055	TTF-DPP-6′–Ti_5O_{10}	2.019	2.054	TTF-QNX-6′–Ti_5O_{10}	2.025	2.035
TTF-PTZ-7′–Ti_5O_{10}	2.032	2.048	TTF-DPP-7′–Ti_5O_{10}	2.016	2.053	TTF-QNX-7′–Ti_5O_{10}	2.023	2.033
TTF-PTZ-8′–Ti_5O_{10}	2.036	2.051	TTF-DPP-8′–Ti_5O_{10}	2.017	2.050	TTF-QNX-8′–Ti_5O_{10}	2.023	2.034

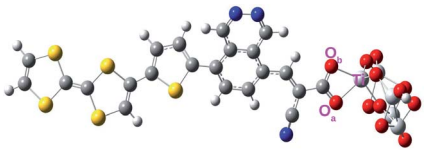

Fig. 9 Representation of the Ti–O bond lengths in the TTF-PTZ–Ti_5O_{10} cluster.

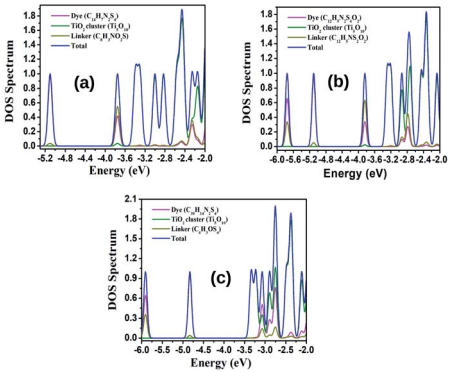

Fig. 10 PDOS spectra of the unsubstituted parent dye clusters (a) TTF-PTZ–Ti_5O_{10}, (b) TTF-DPP–Ti_5O_{10} and (c) TTF-QNX–Ti_5O_{10}.

dye–Ti_5O_{10} clusters. Moreover, from the comparison of Table 5 and Table 9, it is observed that the μ_g values of the dye–Ti_5O_{10} clusters are larger than those of the isolated dyes. These findings suggest that the binding of the dyes to the Ti_5O_{10} semiconducting surface leads to the augmentation of their charge transport properties.

To envisage the correlation of the electronic structure with the frontier molecular orbitals, the PDOS of all of the dye–Ti_5O_{10} clusters have been calculated and their corresponding spectral data are reported in Table S4 (in the ESI†). The PDOS spectra provide a clear view of the nature of the HOMO and LUMO energy levels. The PDOS spectra of the unsubstituted dye–Ti_5O_{10} clusters are given in Fig. 10 and the corresponding spectra for the other dye–Ti_5O_{10} clusters are provided in Fig. S6 (in the ESI†).

From Table S4 (in the ESI†), it is observed that the donor and acceptor units of all dye–Ti_5O_{10} clusters offer the maximum contribution to the HOMOs. On the other hand, the bridging unit and anchoring group offer minimal contribution to the HOMOs. However, the bridging unit and anchoring group of TTF-PTZ–Ti_5O_{10} and TTF-DPP–Ti_5O_{10} and their derivatives offer the maximum contribution to the LUMOs, whereas their donor and acceptor units offer minimal contribution to the LUMOs. Moreover, the Ti_5O_{10} cluster of compounds TTF-PTZ and TTF-DPP and their derivatives have contributed only to the LUMOs, with a maximum of 4% contribution being observed for the compounds TTF-PTZ–Ti_5O_{10}, TTF-PTZ-1–Ti_5O_{10}, TTF-PTZ-2–Ti_5O_{10}, TTF-PTZ-3–Ti_5O_{10}, TTF-PTZ-4–Ti_5O_{10} and TTF-PTZ-5–Ti_5O_{10}. In the case of the compound TTF-QNX and its derivatives, the Ti_5O_{10} cluster offers 100% contribution to the LUMOs, with an exception of only 2% contribution being observed for TTF-QNX-6′–Ti_5O_{10}. Moreover, it has been observed that in compound TTF-QNX and most of its derivatives, the donor and acceptor units, along with the bridging unit and anchoring group, offer no contribution to the LUMOs. However, in case of TTF-QNX-6′–Ti_5O_{10}, the donor and acceptor units, along with the bridging unit and anchoring group, offer contributions of 90% and 8%, respectively, to the LUMOs.

A popular way of visualizing the electrostatic nature of the molecules is through the molecular electrostatic potential surface (MEPS), also known as electrostatic potential energy maps. MEPS is an important tool which gives qualitative information about the charge transportation from the donor moiety to the acceptor moiety.[58,59] It also allows one to visualize the variable charge region of a molecule. The positive potential increases in the following color order: red < orange < yellow < green < blue. Here, the blue color represents the electron-deficient region and the red color represents the electron-rich region. We present the MEPS plots of the unsubstituted dye–Ti_5O_{10} clusters in Fig. 11. For the substituted dye–Ti_5O_{10} clusters, the MEPS plots are presented in Fig. S7 (in the ESI†).

From Fig. 11 and S7,† it is observed that for all of the studied dye–Ti_5O_{10} clusters, the positive charge is spread over the dyes and the negative charge is spread over the Ti_5O_{10} surface, which signifies the charge transfer characteristics of all of the studied dyes.

To further study the absorption properties of the dye–Ti_5O_{10} clusters, we have calculated the excitation energies (E_g),

Table 9 Δ_{H-L} values and μ_g values of the dye–Ti_5O_{10} clusters

Dye–Ti_5O_{10}	Δ_{H-L} (eV)	μ_g (Debye)	Dye–Ti_5O_{10}	Δ_{H-L} (eV)	μ_g (Debye)	Dye–Ti_5O_{10}	Δ_{H-L} (eV)	μ_g (Debye)
TTF-PTZ–Ti_5O_{10}	1.34	11.02	TTF-DPP–Ti_5O_{10}	1.26	14.17	TTF-QNX–Ti_5O_{10}	1.49	12.18
TTF-PTZ-1–Ti_5O_{10}	1.27	12.10	TTF-DPP-1–Ti_5O_{10}	1.19	15.56	TTF-QNX-1–Ti_5O_{10}	1.39	12.58
TTF-PTZ-2–Ti_5O_{10}	1.39	11.72	TTF-DPP-2–Ti_5O_{10}	1.31	14.78	TTF-QNX-2–Ti_5O_{10}	1.57	7.34
TTF-PTZ-3–Ti_5O_{10}	1.20	13.72	TTF-DPP-3–Ti_5O_{10}	1.19	16.18	TTF-QNX-3–Ti_5O_{10}	1.43	7.83
TTF-PTZ-4–Ti_5O_{10}	1.16	12.18	TTF-DPP-4–Ti_5O_{10}	1.09	18.32	TTF-QNX-4–Ti_5O_{10}	1.29	14.65
TTF-PTZ-5–Ti_5O_{10}	1.38	8.05	TTF-DPP-5–Ti_5O_{10}	1.18	15.13	TTF-QNX-5–Ti_5O_{10}	1.50	13.30
TTF-PTZ-6′–Ti_5O_{10}	1.05	10.70	TTF-DPP-6′–Ti_5O_{10}	1.08	11.82	TTF-QNX-6′–Ti_5O_{10}	1.39	10.65
TTF-PTZ-7′–Ti_5O_{10}	1.24	10.42	TTF-DPP-7′–Ti_5O_{10}	1.18	13.81	TTF-QNX-7′–Ti_5O_{10}	1.49	11.50
TTF-PTZ-8′–Ti_5O_{10}	1.14	9.36	TTF-DPP-8′–Ti_5O_{10}	1.18	15.12	TTF-QNX-8′–Ti_5O_{10}	1.50	11.82

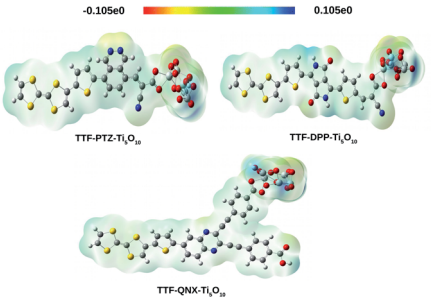

Fig. 11 MEPS contour plots for the three unsubstituted dye–Ti_5O_{10} clusters.

maximum absorption wavelength (λ_{max}), oscillator strengths (f_{osc}), dipole moments (μ), transitions and contribution of the frontier orbitals by employing the CAM-B3LYP functional and these are reported in Table 10.

From Table 10, it is observed that the studied dye–Ti_5O_{10} clusters exhibit an increase in the maximum absorption wavelength (λ_{max}) values with a corresponding decrease in the excitation energies (E_g). This implies red-shift in the adsorbed dyes compared to in the isolated dyes. For TTF-PTZ-6′–Ti_5O_{10}, TTF-DPP-6′–Ti_5O_{10} and TTF-QNX-6′–Ti_5O_{10}, the presence of the $-NO_2$ group at the acceptor part causes the maximum red-shift with the highest λ_{max} values, *viz.*, 562 nm, 657 nm and 476 nm, respectively. On the other hand, the presence of the $-SC_3H_7$ group at the donor part causes a blue shift with a minimum λ_{max} value of 608 nm and 405 nm for TTF-DPP-2–Ti_5O_{10} and TTF-QNX-2–Ti_5O_{10}, respectively. Moreover, in the case of the TTF-PTZ–Ti_5O_{10} cluster and its derivatives, the presence of the –OH group at the donor part causes a blue shift with a minimum λ_{max} value of 494 nm for TTF-PTZ-5–Ti_5O_{10}. We present the plot of the UV–visible spectra of TTF-PTZ–Ti_5O_{10}, TTF-DPP–Ti_5O_{10}, TTF-QNX–Ti_5O_{10} and their derivatives in Fig. 12.

Table 10 E_g, λ_{max}, f_{osc}, transitions and μ of the dye–Ti_5O_{10} clusters

Dye	E_g (eV)	λ_{max} (nm)	f_{osc}	Transition	μ (Debye)
TTF-PTZ–Ti_5O_{10}	2.43	510	0.48	H → L (83%)	11.02
TTF-PTZ-1–Ti_5O_{10}	2.36	525	0.45	H → L (84%)	12.10
TTF-PTZ-2–Ti_5O_{10}	2.48	498	0.55	H → L (79%)	11.72
TTF-PTZ-3–Ti_5O_{10}	2.32	534	0.42	H → L (85%)	13.72
TTF-PTZ-4–Ti_5O_{10}	2.31	535	0.39	H → L (85%)	12.18
TTF-PTZ-5–Ti_5O_{10}	2.50	494	0.52	H → L (80%)	8.05
TTF-PTZ-6′–Ti_5O_{10}	2.20	562	0.24	H → L (89%)	10.70
TTF-PTZ-7′–Ti_5O_{10}	2.29	539	0.45	H → L (86%)	10.42
TTF-PTZ-8′–Ti_5O_{10}	2.36	525	0.25	H → L (89%)	9.36
TTF-DPP–Ti_5O_{10}	2.02	613	1.45	H → L (47%)	14.17
TTF-DPP-1–Ti_5O_{10}	1.99	622	1.42	H → L (50%)	15.56
TTF-DPP-2–Ti_5O_{10}	2.04	608	1.57	H−1 → L (48%)	14.78
TTF-DPP-3–Ti_5O_{10}	2.01	615	1.48	H−1 → L (46%)	16.18
TTF-DPP-4–Ti_5O_{10}	1.98	626	1.34	H → L (49%)	18.32
TTF-DPP-5–Ti_5O_{10}	2.03	612	1.44	H−1 → L (48%)	15.13
TTF-DPP-6′–Ti_5O_{10}	1.88	657	0.80	H → L (79%)	11.82
TTF-DPP-7′–Ti_5O_{10}	2.00	618	1.14	H → L (66%)	13.81
TTF-DPP-8′–Ti_5O_{10}	2.03	610	1.03	H → L (67%)	15.12
TTF-QNX–Ti_5O_{10}	3.00	412	0.98	H → L+3 (35%)	11.73
TTF-QNX-1–Ti_5O_{10}	2.97	417	0.91	H → L+3 (35%)	12.09
TTF-QNX-2–Ti_5O_{10}	3.06	405	1.15	H → L+3 (34%)	6.93
TTF-QNX-3–Ti_5O_{10}	3.00	411	0.85	H → L+3 (31%)	7.23
TTF-QNX-4–Ti_5O_{10}	2.95	420	0.84	H → L+3 (36%)	14.16
TTF-QNX-5–Ti_5O_{10}	3.01	412	0.26	H → L+18 (30%)	12.97
TTF-QNX-6′–Ti_5O_{10}	2.60	476	0.47	H → L (77%)	10.48
TTF-QNX-7′–Ti_5O_{10}	2.92	424	0.95	H → L+3 (44%)	10.99
TTF-QNX-8′–Ti_5O_{10}	2.79	444	0.65	H → L (62%)	11.48

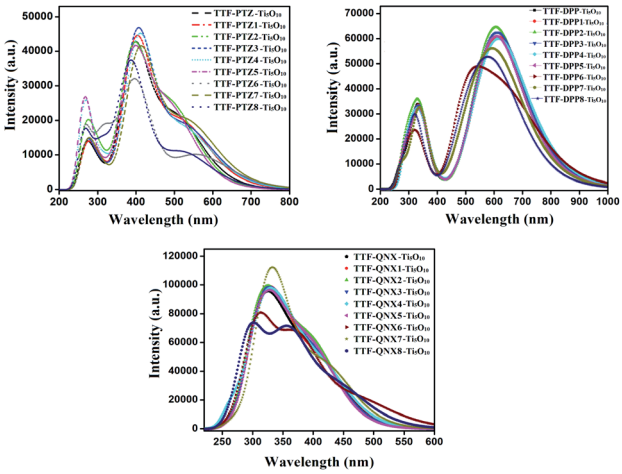

Fig. 12 The plot of the UV–visible spectra of all of the studied dye–Ti_5O_{10} clusters, along with their derivatives.

From the perspective of the electronic transitions and the contribution of the orbitals (Table 10), it is observed that the TTF-PTZ–Ti_5O_{10} cluster and its derivatives undergo transitions from H → L with configurations ranging from 79–89%. Among the TTF-DPP–Ti_5O_{10} cluster and its derivatives, the transitions from H → L with configurations ranging from 47–79% are observed for all except TTF-DPP-2–Ti_5O_{10}, TTF-DPP-3–Ti_5O_{10} and TTF-DPP-5–Ti_5O_{10}, where the predominant transitions are H−1 → L in nature with configurations ranging from 46–48%. Moreover, in the case of the TTF-QNX–Ti_5O_{10} cluster and its derivatives, the dominant transitions are H → L+3 in nature with configurations ranging from 31–44%, except for TTF-QNX-5–Ti_5O_{10}, TTF-QNX-6′–Ti_5O_{10} and TTF-QNX-8′–Ti_5O_{10}. In TTF-QNX-5–Ti_5O_{10}, the transition is from H → L+18 with 30% configuration. On the other hand, in the case of TTF-QNX-6′–Ti_5O_{10} and TTF-QNX-8′–Ti_5O_{10}, the dominant transitions occur from H → L with 77% and 62% of configurations respectively.

4.8 Exciton binding energy (EBE) calculations and electron density difference (EDD) maps of the dye–TiO_2 clusters

Exciton binding energy (EBE) is an important aspect for the efficiency of solar cells. It is directly related to the charge separation in excitonic solar cells.[60] The working mechanism of DSSCs is simply that sunlight is absorbed by the dye molecule to produce an exciton, *i.e.*, an electron–hole pair, which further splits after the exciton reaches the TiO_2 semiconducting surface. In this regard, the amount of energy required to pull apart the electron and hole from an exciton is known as the exciton binding energy (EBE).[55,61] The lower the EBE value, the easier the charge separation from the dye molecule to the

Table 11 Exciton binding energy (EBE) values of the dye–Ti_5O_{10} clusters

Dye–Ti_5O_{10}	E_b (eV)	Dye–Ti_5O_{10}	E_b (eV)	Dye–Ti_5O_{10}	E_b (eV)
TTF-PTZ–Ti_5O_{10}	1.20	TTF-DPP–Ti_5O_{10}	1.36	TTF-QNX–Ti_5O_{10}	1.07
TTF-PTZ-1–Ti_5O_{10}	1.18	TTF-DPP-1–Ti_5O_{10}	1.31	TTF-QNX-1–Ti_5O_{10}	1.00
TTF-PTZ-2–Ti_5O_{10}	1.23	TTF-DPP-2–Ti_5O_{10}	1.43	TTF-QNX-2–Ti_5O_{10}	1.13
TTF-PTZ-3–Ti_5O_{10}	1.21	TTF-DPP-3–Ti_5O_{10}	1.33	TTF-QNX-3–Ti_5O_{10}	1.05
TTF-PTZ-4–Ti_5O_{10}	1.13	TTF-DPP-4–Ti_5O_{10}	1.23	TTF-QNX-4–Ti_5O_{10}	0.95
TTF-PTZ-5–Ti_5O_{10}	1.19	TTF-DPP-5–Ti_5O_{10}	1.37	TTF-QNX-5–Ti_5O_{10}	1.10
TTF-PTZ-6′–Ti_5O_{10}	1.12	TTF-DPP-6′–Ti_5O_{10}	1.25	TTF-QNX-6′–Ti_5O_{10}	1.09
TTF-PTZ-7′–Ti_5O_{10}	1.18	TTF-DPP-7′–Ti_5O_{10}	1.27	TTF-QNX-7′–Ti_5O_{10}	0.89
TTF-PTZ-8′–Ti_5O_{10}	1.08	TTF-DPP-8′–Ti_5O_{10}	1.28	TTF-QNX-8′–Ti_5O_{10}	1.14

semiconducting surface. The EBE can be considered to be the difference between the electronic and optical band gap energies, *i.e.*, $E_b = \Delta_{H-L} - E_1$, where E_1 is the energy required for the $S_0 \rightarrow S_1$ transition.[62,63] The corresponding EBE values of all of the dye–Ti_5O_{10} clusters are given in Table 11.

From Table 11, it is observed that all the dye–Ti_5O_{10} clusters exhibit low E_b values. However, the dye clusters TTF-PTZ-8′–Ti_5O_{10}, TTF-DPP-4–Ti_5O_{10} and TTF-QNX-7′–Ti_5O_{10} exhibit relatively lower E_b values than the rest, indicating the occurrence of facile charge separation. Among the dye–Ti_5O_{10} clusters, TTF-QNX–Ti_5O_{10} and its derivatives exhibit comparatively lower E_b values than those of the other two groups of dye clusters. This implies that the transfer of electrons from the dye to the Ti_5O_{10} semiconducting surface will be easier in these dye clusters. On the other hand, the dye cluster TTF-DPP-2–Ti_5O_{10} exhibits the maximum E_b value, which in turn leads to a comparatively difficult charge separation.

To further study the intramolecular charge transfer (ICT) that takes place during the $S_0 \rightarrow S_1$ transition, we have performed an efficient analysis of the electronic structures of the dye–Ti_5O_{10} clusters. The EDD maps of the unsubstituted parent dye–Ti_5O_{10} clusters are presented in Fig. 13 and those for the rest of the dyes are provided in Fig. S8 (in the ESI†). In Fig. 13 and S8,† green and blue regions correspond to the increase and decrease in electron density due to the excitation of electrons during the $S_0 \rightarrow S_1$ transition, respectively.

From Fig. 13, it is observed that the Ti_5O_{10} cluster exhibits the maximum electron density and the donor unit exhibits the minimum electron density. This in turn implies that the charge transfer occurs from the dye to the TiO_2 semiconducting surface during the $S_0 \rightarrow S_1$ transition.

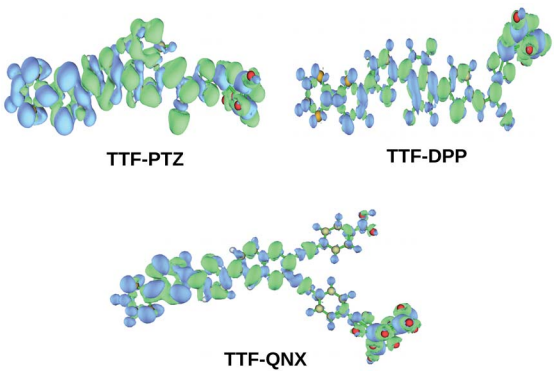

Fig. 13 Electron density difference (EDD) maps of the unsubstituted parent dye–Ti_5O_{10} clusters.

5. Conclusion

We have performed a detailed theoretical study to gather information regarding the optoelectronic properties of three designed groups of dyes, *viz.*, TTF-DPP, TTF-QNX and TTF-PTZ. To study their structural and electronic properties, we have calculated the dihedral angles, Δ_{H-L} values, spectral data from PDOS spectra and μ values of the designed dyes. From the observed Δ_{H-L} values of the dyes, it can be revealed that the dyes TTF-DPP-4 and TTF-DPP-6′ possess the lowest Δ_{H-L} values. Moreover, the attachment of the $-NH_2$ group at the donor unit and the $-NO_2$ and $-CF_3$ groups at the acceptor units lower the Δ_{H-L} values of all of the designed dyes. In addition, the spectral data obtained from the PDOS demonstrate that the attachment of electron donating groups at the donor part increases the contribution of the donor unit to the HOMO energy level. It is also evident that the GSOPs of all the designed dyes lie below the redox potential of the I^-/I_3^- electrolyte couple. However, the ESOPs of the TTF-PTZ and TTF-QNX groups of dyes, along with those of most of the dyes belonging to TTF-DPP group, lie above the conduction band of the TiO_2 semiconducting surface. From the ΔG^{inj} and ΔG^{reg} values, it is evident that the dyes TTF-PTZ-4 and TTF-DPP-4, along with the TTF-QNX group of dyes, may act as suitable candidates for the fabrication of DSSCs. Moreover, the observed values of IP and EA suggest that the TTF-QNX group of dyes are better candidates for the construction of DSSCs. The obtained λ_{tot} values also confirm the better efficiency of electron–hole separation in the TTF-DPP and TTF-QNX groups of dyes. From the absorption properties of the designed dyes, it is evident that the TTF-DPP group of dyes possess the maximum λ_{max} values and attachment of the $-CH_3$ group at the donor part further increases the electron density of TTF-DPP-1, which leads to the maximum red-shift. Furthermore, the EDD maps confirm that the $S_0 \rightarrow S_1$ transition involves greater charge transfer from the donor unit to the acceptor unit for all of the designed dyes. Hence, we can conclude that our designed dyes can serve as potential candidates for the fabrication of DSSCs.

From the study of the structural and electronic properties of the designed dye–Ti_5O_{10} clusters, it can be inferred that the μ_g

values are high for all of the dye–Ti_5O_{10} clusters, with a decrease in the Δ_{H-L} values compared to those of the isolated dyes. This confirms the enhancement of the charge transport properties of the designed dyes upon binding the dye to the Ti_5O_{10} semiconducting surface. Moreover, the absorption spectra of the dye–Ti_5O_{10} clusters confirm an increase in the maximum absorption wavelength (λ_{max}) values with a corresponding decrease in the excitation energies (E_g), implying the occurrence of red-shift compared to the isolated dyes. As a result, the performance of the dyes is increased upon binding to the TiO_2 surface. In short, we can conclude that most of the designed dyes may act as potential candidates for the fabrication of DSSCs.

Conflicts of interest

There are no conflicts to declare.

Acknowledgements

The authors would like to acknowledge the Department of Science and Technology (SB/FT/CS-077/2013), India for the financial support. The authors would like to acknowledge the University Grants Commission for UGC-BSR Research start-up-grant (NO.F.30.-122/2015(BSR)), Gauhati University for providing the research facilities and financial support. The author would also like to acknowledge Dr Rakesh Dutta, Ms Shahnaz Ahmed and Ms Suranjana Patowary for their help in the manuscript preparation.

Notes and references

1 C.-R. Lee, H.-S. Kim, I.-H. Jang, J.-H. Im and N.-G. Park, *ACS Appl. Mater. Interfaces*, 2011, **3**, 1953–1957.
2 B. E. Hardin, H. J. Snaith and M. D. McGehee, *Nat. Photonics*, 2012, **6**, 162–169.
3 R. K. Kanaparthi, J. Kandhadi and L. Giribabu, *Tetrahedron*, 2012, **68**, 8383–8393.
4 Y. Akila, N. Muthukumarasamy and D. Velauthapillai, *Nanomater. Sol. Cell Appl.*, 2019, 127–144.
5 S. Shalini, S. Prasanna, T. K. Mallick and S. Senthilarasu, *Renewable Sustainable Energy Rev.*, 2015, **51**, 1306–1325.
6 Ö. Birel, *Electron. J. Vocat. Coll.*, 2015, **5**, 89–98.
7 N. N. Ghosh, A. Chakraborty, S. Pal, A. Pramanik and P. Sarkar, *Phys. Chem. Chem. Phys.*, 2014, **16**, 25280–25287.
8 M. Grätzel, *Acc. Chem. Res.*, 2009, **42**, 1788–1798.
9 L. Zhang and J. M. Cole, *ACS Appl. Mater. Interfaces*, 2015, **7**, 3427–3455.
10 K. Sharma, V. Sharma and S. Sharma, *Nanoscale Res. Lett.*, 2018, **13**, 381.
11 C. Teng, X. Yang, S. Li, M. Cheng, A. Hagfeldt, L.-z. Wu and L. Sun, *Chem.–Eur. J.*, 2010, **16**, 13127–13138.
12 C.-P. Hsieh, H.-P. Lu, C.-L. Chiu, C.-W. Lee, S.-H. Chuang, C.-L. Mai, W.-N. Yen, S.-J. Hsu, E. W.-G. Diau and C.-Y. Yeh, *J. Mater. Chem.*, 2010, **20**, 1127–1134.
13 A. Karuppasamy, K. Stalindurai, J.-D. Peng, K.-C. Ho and C. Ramalingan, *Phys. Chem. Chem. Phys.*, 2016, **18**, 30105–30116.
14 C. Teng, X. Yang, C. Yang, S. Li, M. Cheng, A. Hagfeldt and L. Sun, *J. Phys. Chem. C*, 2010, **114**, 9101–9110.
15 X. Zhao and X. Zhan, *Chem. Soc. Rev.*, 2011, **40**, 3728–3743.
16 R. Stalder, J. Mei, K. R. Graham, L. A. Estrada and J. R. Reynolds, *Chem. Mater.*, 2014, **26**, 664–678.
17 S. Hwang, J. H. Lee, C. Park, H. Lee, C. Kim, C. Park, M.-H. Lee, W. Lee, J. Park, K. Kim, N.-G. Park and C. Kim, *Chem. Commun.*, 2007, **2007**(46), 4887–4889.
18 K. Hara, T. Sato, R. Katoh, A. Furube, Y. Ohga, A. Shinpo, S. Suga, K. Sayama, H. Sugihara and H. Arakawa, *J. Phys. Chem. B*, 2003, **107**, 597–606.
19 A. Amacher, C. Yi, J. Yang, M. P. Bircher, Y. Fu, M. Cascella, M. Grätzel, S. Decurtins and S.-X. Liu, *Chem. Commun.*, 2014, **50**, 6540–6542.
20 K. Sayama, K. Hara, N. Mori, M. Satsuki, S. Suga, S. Tsukagoshi, Y. Abe, H. Sugihara and H. Arakawa, *Chem. Commun.*, 2000, **2000**(13), 1173–1174.
21 X. Ma, J. Hua, W. Wu, Y. Jin, F. Meng, W. Zhan and H. Tian, *Tetrahedron*, 2008, **64**, 345–350.
22 T. Horiuchi, H. Miura, K. Sumioka and S. Uchida, *J. Am. Chem. Soc.*, 2004, **126**, 12218–12219.
23 Z.-S. Wang, F.-Y. Li and C.-H. Huang, *J. Phys. Chem. B*, 2001, **105**, 9210–9217.
24 S. Ferrere, A. Zaban and B. A. Gregg, *J. Phys. Chem. B*, 1997, **101**, 4490–4493.
25 T. Kitamura, M. Ikeda, K. Shigaki, T. Inoue, N. A. Anderson, X. Ai, T. Lian and S. Yanagida, *Chem. Mater.*, 2004, **16**, 1806–1812.
26 S.-L. Li, K.-J. Jiang, K.-F. Shao and L.-M. Yang, *Chem. Commun.*, 2006, **2006**(26), 2792–2794.
27 H. Tian, X. Yang, R. Chen, Y. Pan, L. Li, A. Hagfeldt and L. Sun, *Chem. Commun.*, 2007, **36**(36), 3741–3743.
28 R. Chen, X. Yang, H. Tian, X. Wang, A. Hagfeldt and L. Sun, *Chem. Mater.*, 2007, **19**, 4007–4015.
29 D. Kim, J. K. Lee, S. O. Kang and J. Ko, *Tetrahedron*, 2007, **63**, 1913–1922.
30 J. L. Segura and N. Martin, *Angew. Chem., Int. Ed.*, 2001, **40**, 1372–1409.
31 F. Pop, J. Ding, L. M. L. Daku, A. Hauser and N. Avarvari, *R. Soc. Chem. Adv.*, 2013, **3**, 3218–3221.
32 S. Wenger, P.-A. Bouit, Q. Pierre-Antoine, J. Teuscher, D. D. Censo, R. H. Baker, J.-E. Moser, J. L. Delgado, N. Martı, S. M. Zakeeruddin and M. Gratzel, *J. Am. Chem. Soc.*, 2010, **132**, 5164–5169.
33 K. Guo, K. Yan, X. Lu, Y. Qiu, Z. Liu, J. Sun, F. Yan, W. Guo and S. Yang, *Org. Lett.*, 2012, **14**, 2214–2217.
34 L. Giribabu, N. Duvva, S. P. Singh, L. Han, I. M. Bedja, R. K. Gupta and A. Islam, *Mater. Chem. Front.*, 2017, **1**, 460–467.
35 L. Giribabu, N. Duvva, S. Prasanthkumar, S. P. Singh, L. Han, I. Bedja, R. K. Gupta and A. Islam, *Sustainable Energy Fuels*, 2017, **1**, 345–353.
36 W. Fan, D. Tan, Q. Zhang and H. Wang, *J. Mol. Graphics Modell.*, 2015, **57**, 62–69.

37 X. Li, Y. Hu, I. Sanchez-Molina, Y. Zhou, F. Yu, S. A. Haque, W. Wu, J. Hua, H. Tian and N. Robertson, *J. Mater. Chem. A*, 2015, **3**, 21733–21743.
38 M. Frisch, G. Trucks, H. Schlegel, G. Scuseria, M. Robb, J. Cheeseman, G. Scalmani, V. Barone, B. Mennucci, G. Petersson *et al.*, *Gaussian 09, Revision E. 01*, Gaussian, Wallingford CT, 2009, vol. 121, pp. 150–166.
39 R. Dutta, S. Ahmed and D. J. Kalita, *Mater. Today Commun.*, 2020, **22**, 100731.
40 H. Sahu and A. N. Panda, *Phys. Chem. Chem. Phys.*, 2014, **16**, 8563–8574.
41 L. L. Estrella, M. P. Balanay and D. H. Kim, *J. Phys. Chem. A*, 2016, **120**, 5917–5927.
42 T. Sutradhar and A. Misra, *J. Phys. Chem. A*, 2018, **122**, 4111–4120.
43 S. Ahmed, B. C. Mushahary and D. J. Kalita, *ACS Omega*, 2020, **5**, 8321–8333.
44 Q. S. Yin, H. JianLi and T. He, *Sci. China: Chem.*, 2012, **55**, 1314–1318.
45 L. Zhang and J. M. Cole, *ACS Appl. Mater. Interfaces*, 2015, **7**, 3427–3455.
46 S. Zhang, X. Yang, Y. Numata and L. Han, *Energy Environ. Sci.*, 2013, **6**, 1443–1464.
47 W. Sang-aroon, S. Saekow and V. Amornkitbamrung, *J. Photochem. Photobiol., A*, 2012, **236**, 35–40.
48 L. L. Estrella, M. P. Balanay and D. H. Kim, *J. Phys. Chem. A*, 2016, **120**, 5917–5927.
49 F. De Angelis, S. Fantacci and A. Selloni, *Nanotechnology*, 2008, **19**, 1–7.
50 F. Manzoor, J. Iqbal, Z. Zara, B. Eliasson, M. S. Mahr and K. Ayub, *ChemistrySelect*, 2018, **3**, 1593–1601.
51 Y. Wen, W. Zhang, X. Zhu, J. Zhang and L. Wang, *Energy*, 2018, **158**, 537–545.
52 S. Muhammad, M. Nakano, A. G. Al-Sehemi, A. Irfan, A. R. Chaudhry, T. Tonami, S. Ito, R. Kishi and Y. Kitagawa, *Nanoscale*, 2018, **10**, 16499–16507.
53 X.-H. Xie, X.-W. Zhao and M. Li, *Int. J. Polym. Sci.*, 2018, **2018**, 1–11.
54 T. Lu and F. Chen, *J. Comput. Chem.*, 2012, **33**, 580–592.
55 G. Gogoi, L. Bhattacharya, S. Rahman, N. S. Sarma, S. Sahu, B. K. Rajbongshi and S. Sharma, *Mater. Today Commun.*, 2020, **25**, 101364.
56 S. Ahmed, S. R. Bora, T. Chutia and D. J. Kalita, *Phys. Chem. Chem. Phys.*, 2021, **23**, 13190–13203.
57 Y. Jiao, F. Zhang, M. Grätzel and S. Meng, *Adv. Funct. Mater.*, 2013, **23**, 424–429.
58 M. M. Raikwar, D. S. Patil, E. Mathew, M. Varghese, I. H. Joe and N. Sekar, *J. Photochem. Photobiol., A*, 2019, **373**, 45–58.
59 M. Zouaoui-Rabah, M. Sekkal-Rahal, F. Djilani-Kobibi, A. M. Elhorri and M. Springborg, *J. Phys. Chem. A*, 2016, **120**, 8843–8852.
60 R. A. Marcus and N. Sutin, *Biochim. Biophys. Acta, Rev. Bioenerg.*, 1985, **811**, 265–322.
61 P. K. Nayak, *Synth. Met.*, 2013, **174**, 42–45.
62 Y.-L. Wang, Q.-S. Li and Z.-S. Li, *Comput. Mater. Sci.*, 2019, **156**, 252–259.
63 Y.-L. Wang, Q.-S. Li and Z.-S. Li, *Phys. Chem. Chem. Phys.*, 2017, **19**, 23444–23453.